Self-Assembly, Molecular Ordering, and Charge Mobility in Solution-Processed Ultrathin Oligothiophene Films

Amanda R. Murphy,[†,‡] Paul C. Chang,[†,§] Priscilla VanDyke,[‡] Jinsong Liu,[†,‡] Jean M. J. Fréchet,*[,†,‡] Vivek Subramanian,[†,§] Dean M. DeLongchamp,[||] Sharadha Sambasivan,[||] Daniel A. Fischer,[||] and Eric K. Lin[||]

Material Sciences Division, Lawrence Berkeley National Laboratory, Berkeley, California, Department of Chemistry and Department of Electrical Engineering and Computer Sciences, University of California, Berkeley, California 94720-1460, and Polymers Division, National Institute of Standards and Technology, Gaithersburg, Maryland 20899

Received July 14, 2005. Revised Manuscript Received September 24, 2005

Symmetrical α,ω-substituted quarter-(**T4**), penta-(**T5**), sexi-(**T6**), and heptathiophene (**T7**) oligomers containing thermally removable aliphatic ester solubilizing groups were synthesized, and their UV−vis and thermal characteristics were compared. Spun-cast thin films of each oligomer were examined with atomic force microscopy and near-edge X-ray absorption fine structure spectroscopy to evaluate the ability of the material to self-assemble from a solution-based process while maintaining complete surface coverage. Films of the **T5**−**T7** oligomers self-assemble into crystalline terraces after thermal annealing with higher temperatures required to affect this transformation as the size of the oligomers increases. A symmetrical α,ω-substituted sexithiophene (**T6-acid**) that reveals carboxylic acids after thermolysis was also prepared to evaluate the effect of the presence of hydrogen-bonding moieties. The charge transport properties for these materials evaluated in top-contact thin film transistor devices were found to correlate with the observed morphology of the films. Therefore, the **T4** and the **T6-acid** performed poorly because of incomplete surface coverage after thermolysis, while **T5**−**T7** exhibited much higher performance as a result of molecular ordering. Increases in charge mobility correlated to increasing conjugation length with measured mobilities ranging from 0.02 to 0.06 $cm^2/(V \cdot s)$. The highest mobilities were measured when films of each oligomer had an average thickness between one and two monolayers, indicating that the molecules become exceptionally well-ordered during the thermolysis process. This unprecedented ordering of the solution-cast molecules results in efficient charge mobility rarely seen in such ultrathin films.

Introduction

It is well-known that efficient organic semiconductors require a high degree of molecular organization involving extended π-stacked or herringbone networks to achieve efficient charge mobility.[1−4] These strong π interactions in the highest performance organic semiconductors such as pentacene,[5−7] oligothiophene derivatives,[8−15] and hybrid conjugated oligomers[16−25] decreases the solubility, and, thus, the use of thermal evaporation is needed to obtain thin films. While this processing technique is expensive and time-

* To whom correspondence should be addressed. E-mail: frechet@berkeley.edu.
† Lawrence Berkeley National Laboratory.
‡ Department of Chemistry, University of California.
§ Department of Electrical Engineering and Computer Sciences, University of California.
|| National Institute of Standards and Technology.

(1) Dimitrakopoulos, C. D.; Malenfant, P. R. L. *Adv. Mater.* **2002**, *14*, 99−117.
(2) Katz, H. E. *Chem. Mater.* **2004**, *16*, 4748−4756.
(3) Ling, M. M.; Bao, Z. *Chem. Mater.* **2004**, *16*, 4824−4840.
(4) Newman, C. R.; Frisbie, C. D.; Silva Filho, D. A.; Bredas, J. L.; Ewbank, P. C.; Mann, K. R. *Chem. Mater.* **2004**, *16*, 4436−4451.
(5) Dimitrakopoulos, C. D.; Brown, A. R.; Pomp, A. *J. Appl. Phys.* **1996**, *80*, 2501−2508.
(6) Garnier, F.; Horowitz, G.; Peng, X. Z.; Fichou, D. *Synth. Met.* **1991**, *45*, 163−171.
(7) Laquindanum, J. G.; Katz, H. E.; Lovinger, A. J.; Dodabalapur, A. *Chem. Mater.* **1996**, *8*, 2542−2544.
(8) Fichou, D. *Handbook of Oligo- and Polythiophenes*; Wiley-VCH: New York, 1998.
(9) Fichou, D. *J. Mater. Chem.* **2000**, *10*, 571−588.
(10) Garnier, F.; Yassar, A.; Hajlaoui, R.; Horowitz, G.; Deloffre, F.; Servet, B.; Ries, S.; Alnot, P. *J. Am. Chem.* Soc. **1993**, *115*, 8716−8721.
(11) Meng, H.; Zheng, J.; Lovinger, A. J.; Wang, B. C.; Van Patten, P. G.; Bao, Z. N. *Chem. Mater.* **2003**, *15*, 1778−1787.
(12) Servet, B.; Horowitz, G.; Ries, S.; Lagorsse, O.; Alnot, P.; Yassar, A.; Deloffre, F.; Srivastava, P.; Hajlaoui, R.; Lang, P.; Garnier, F. *Chem. Mater.* **1994**, *6*, 1809−1815.
(13) Halik, M.; Klauk, H.; Zschieschang, U.; Schmid, G.; Ponomarenko, S.; Kirchmeyer, S.; Weber, W. *Adv. Mater.* **2003**, *15*, 917−923.
(14) Locklin, J.; Li, D.; Mannsfeld, S. C. B.; Borkent, E. J.; Meng, H.; Advincula, R.; Bao, Z. *Chem. Mater.* **2005**, *17*, 3366−3374.
(15) Yoon, M. H.; DiBenedetto, S. A.; Facchetti, A.; Marks, T. J. *J. Am. Chem. Soc.* **2005**, *127*, 1348−1349.
(16) Meng, H.; Sun, F.; Goldfinger, M. B.; Jaycox, G. D.; Li, Z.; Marshall, W. J.; Blackman, G. S. *J. Am. Chem. Soc.* **2005**, *127*, 2406−2407.
(17) Merlo, J. A.; Newman, C. R.; Gerlach, C. P.; Kelley, T. W.; Muyres, D. V.; Fritz, S. E.; Toney, M. F.; Frisbie, C. D. *J. Am. Chem. Soc.* **2005**, *127*, 3997−4009.
(18) Nicolas, Y.; Blanchard, P.; Roncali, J.; Allain, M.; Mercier, N.; Deman, A. L.; Tardy, J. *Org. Lett.* **2005**, *7*, 3513−3516.
(19) Ponomarenko, S. A.; Kirchmeyer, S.; Halik, M.; Klauk, H.; Zschieschang, U.; Schmid, G.; Karbach, A.; Drechsler, D.; Alpatova, N. M. *Synth. Met.* **2005**, *149*, 231−235.
(20) Roy, V. A. L.; Zhi, Y. G.; Xu, Z. X.; Yu, S. C.; Chan, P. W. H.; Che, C. M. *Adv. Mater.* **2005**, *17*, 1258.
(21) Takimiya, K.; Kunugi, Y.; Konda, Y.; Niihara, N.; Otsubo, T. *J. Am. Chem. Soc.* **2004**, *126*, 5084−5085.
(22) Takimiya, K.; Kunugi, Y.; Toyoshima, Y.; Otsubo, T. *J. Am. Chem. Soc.* **2005**, *127*, 3605−3612.
(23) Ando, S.; Nishida, J. I.; Fujiwara, E.; Tada, H.; Inoue, Y.; Tokito, S.; Yamashita, Y. *Chem. Mater.* **2005**, *17*, 1261−1264.

10.1021/cm0515350 CCC: $30.25
Published on Web 11/05/2005

consuming, it provides a high degree of control where variables such as time, temperature, and pressure can be optimized to give films with precise thickness and molecular orientation.[1,26] In contrast, very little control over film organization is normally achieved with solution-processed materials. Thus, most materials processed in this manner offer lower performance than their insoluble counterparts.[27−35] To benefit from the extreme cost advantages of solution processing methods such as spin coating,[36,37] stamping,[38,39] or inkjet printing,[40,41] materials must be designed to organize spontaneously. Control of the assembly of oligothiophenes from solution has been attempted through the use of substituents, but the large saturated side chains that are typically used tend to inhibit overall charge transfer through the materials.[42−44] Recently, elegant methods for solubilizing pentacene without dramatically decreasing performance have been demonstrated either by using a precursor route[28,45] or by strategic placement of substituents.[46] However, few reports have focused on structure−property relationships of solution-processed oligothiophenes.[47]

In this work, control of molecular self-assembly from solution using minimal substitution was explored through the synthesis and evaluation of a series of symmetrical α,ω-substituted quarter-, penta-, and heptathiophene oligomers containing thermally removable solubilizing groups, analogous to a sexithiophene derivative we reported previously (Scheme 1).[48,49] This solution-processed sexithiophene was found to have a strong tendency to self-assemble into crystalline terraces after thermal removal of its bulky solubilizing groups. In this work, the use of smaller oligomers for solution-based methods was investigated to explore the structure−property relationships with an emphasis on the ability of the various oligomers to self-assemble. A larger heptathiophene oligomer was also synthesized to establish if increased conjugation length has an influence on the self-assembly leading to a further increase in the charge mobility. In addition, a complementary α,ω-substituted sexithiophene that reveals carboxylic acid end groups after thermolysis was also synthesized and evaluated to explore the effect of hydrogen-bonding moieties on the self-assembling properties of these materials (Scheme 1). The UV−vis and thermal characterization of the bulk materials, along with atomic force microscopy (AFM) and near-edge X-ray absorption fine structure (NEXAFS) spectroscopy of solution-processed films of the series of oligomers, is presented. Different film morphologies were found to correlate with hole mobility when the materials were employed as the active layer in thin film transistor (TFT) devices.

Scheme 1. Oligothiophenes Studied that Produce either Alkenes or Carboxylic Acids after Ester Thermolysis

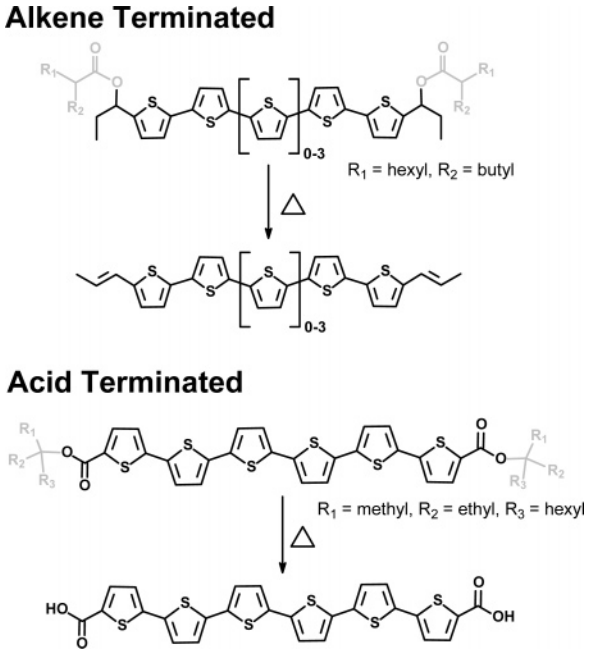

Results and Discussion

Synthesis. The **T4**−**T7** oligomer series was synthesized as shown in Scheme 2. **T4** was generated by Suzuki homocoupling of functionalized bithiophene **1**.[49] Stille cross-coupling of **1** with 2,5-bis(trimethylstannyl)thiophene and 5,5′-bis(tributylstannyl)-2,2′-bithiophene was employed to

(24) Facchetti, A.; Letizia, J.; Yoon, M. H.; Mushrush, M.; Katz, H. E.; Marks, T. J. *Chem. Mater.* **2004**, *16*, 4715−4727.
(25) Facchetti, A.; Mushrush, M.; Yoon, M. H.; Hutchison, G. R.; Ratner, M. A.; Marks, T. J. *J. Am. Chem.* Soc. **2004**, *126*, 13859−13874.
(26) Forrest, S. R. *Chem. Rev.* **1997**, *97*, 1793−1896.
(27) Afzali, A.; Breen, T. L.; Kagan, C. R. *Chem. Mater.* **2002**, *14*, 1742−1746.
(28) Afzali, A.; Dimitrakopoulos, C. D.; Breen, T. L. *J. Am. Chem. Soc.* **2002**, *124*, 8812−8813.
(29) Garnier, F.; Hajlaoui, R.; El Kassmi, A.; Horowitz, G.; Laigre, L.; Porzio, W.; Armanini, M.; Provasoli, F. *Chem. Mater.* **1998**, *10*, 3334−3339.
(30) Katz, H. E.; Laquindanum, J. G.; Lovinger, A. J. *Chem. Mater.* **1998**, *10*, 633−638.
(31) Katz, H. E.; Li, W.; Lovinger, A. J.; Laquindanum, J. *Synth. Met.* **1999**, *102*, 897−899.
(32) Mushrush, M.; Facchetti, A.; Lefenfeld, M.; Katz, H. E.; Marks, T. J. *J. Am. Chem. Soc.* **2003**, *125*, 9414−9423.
(33) Ponomarenko, S. A.; Kirchmeyer, S.; Elschner, A.; Huisman, B. H.; Karbach, A.; Drechsler, D. *Adv. Funct. Mater.* **2003**, *13*, 591−596.
(34) Mushrush, M.; Facchetti, A.; Lefenfeld, M.; Katz, H. E.; Marks, T. J. *J. Am. Chem. Soc.* **2003**, *125*, 9414−9423.
(35) Sun, Y.; Xiao, K.; Liu, Y.; Wang, J.; Pei, J.; Yu, G.; Zhu, D. *Adv. Funct. Mater.* **2005**, *15*, 818−822.
(36) Garnier, F.; Hajlaoui, R.; Yassar, A.; Srivastava, P. *Science* **1994**, *265*, 1684−1686.
(37) Sirringhaus, H.; Tessler, N.; Friend, R. H. *Science* **1998**, *280*, 1741−1744.
(38) Rogers, J. A.; Bao, Z.; Meier, M.; Dodabalapur, A.; Schueller, O. J. A.; Whitesides, G. M. *Synth. Met.* **2000**, *115*, 5−11.
(39) Rogers, J. A.; Bao, Z.; Baldwin, K.; Dodabalapur, A.; Crone, B.; Raju, V. R.; Kuck, V.; Katz, H.; Amundson, K.; Ewing, J.; Drzaic, P. *Proc. Natl. Acad. Sci. U.S.A.* **2001**, *98*, 4835−4840.
(40) Sirringhaus, H.; Kawase, T.; Friend, R. H.; Shimoda, T.; Inbasekaran, M.; Wu, W.; Woo, E. P. *Science* **2000**, *290*, 2123−2126.
(41) Speakman, S. P.; Rozenburg, G. G.; Clay, K. J.; Milne, W. I.; Ille, A.; Gardner, I. A.; Bresler, E.; Steinke, J. H. G. *Org. Electron.* **2001**, *2*, 65−73.
(42) Azumi, R.; Gotz, G.; Bauerle, P. *Synth. Met.* **1999**, *101*, 569−572.
(43) Jiang, L.; Hughes, R. C.; Sasaki, D. Y. *Chem. Commun.* **2004**, 1028−1029.
(44) Sandberg, H.; Henze, O.; Kilbinger, A. F. M.; Sirringhaus, H.; Feast, W. J.; Friend, R. H. *Synth. Met.* **2003**, *137*, 885−886.
(45) Herwig, P. T.; Mullen, K. *Adv. Mater.* **1999**, *11*, 480−483.
(46) Payne, M. M.; Parkin, S. R.; Anthony, J. E.; Kuo, C. C.; Jackson, T. N. *J. Am. Chem. Soc.* **2005**, *127*, 4986−4987.
(47) Katz, H. E.; Siegrist, T.; Lefenfeld, M.; Gopalan, P.; Mushrush, M.; Ocko, B.; Gang, O.; Jisrawl, N. *J. Phys. Chem. B* **2004**, *108*, 8567−8571.
(48) Chang, P. C.; Lee, J.; Huang, D.; Subramanian, V.; Murphy, A. R.; Fréchet, J. M. J. *Chem. Mater.* **2004**, *16*, 4783−4789.
(49) Murphy, A. R.; Fréchet, J. M. J.; Chang, P.; Lee, J.; Subramanian, V. *J. Am. Chem. Soc.* **2004**, *126*, 1596−1597.

Scheme 2. Synthesis of α,ω-Branched Ester Functionalized T4−T7 Oligothiophenes

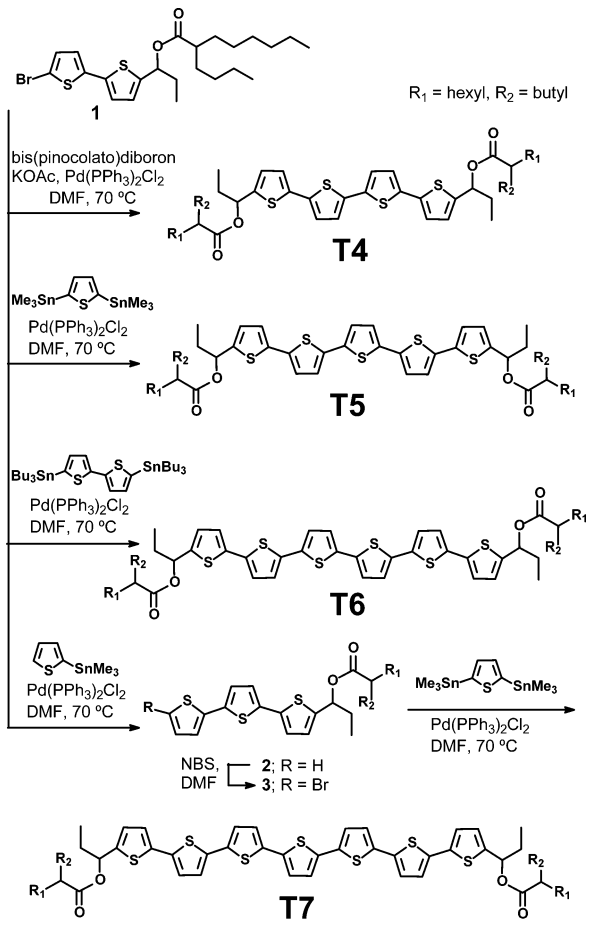

Scheme 3. Synthesis of the T6-acid Precursor Oligothiophene

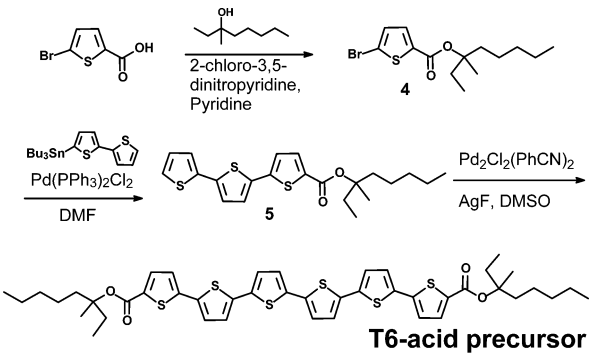

give **T5** and **T6**, respectively. To obtain the **T7** oligomer, an additional thiophene ring was added to **1** by a Stille cross-coupling reaction with 2-(trimethylstannyl)thiophene. Bromination of **2** with *N*-bromosuccinimide to give **3**, followed by cross-coupling with 2,5-bis(trimethylstannyl)thiophene, produced the desired **T7** oligomer. An octathiophene oligomer was also synthesized in an analogous fashion, but its low solubility precluded further investigation of its properties.

The **T6-acid** precursor was synthesized in three steps, as shown in Scheme 3. Esterification of commercially available 2-bromo-5-thiophene carboxylic acid, followed by Stille cross-coupling with 5-(tributylstannyl)-2,2′-bithiophene, afforded terthiophene **5**. The final product was generated using a recently reported homocoupling method utilizing $PdCl_2(PhCN)_2$ and silver fluoride.[50]

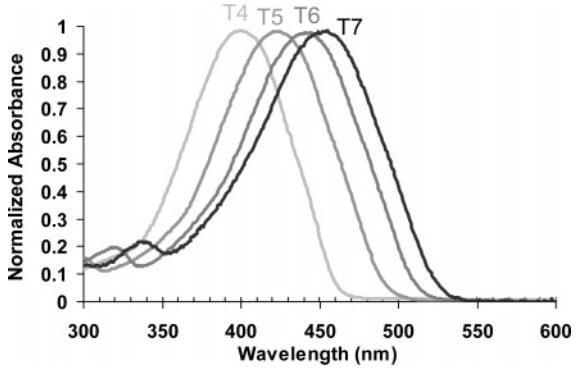

Figure 1. UV−vis spectra of the **T4**−**T7** series in chloroform. The compounds exhibited an increase in λ_{max} from 400 nm for the **T4** to 455 nm for the **T7**.

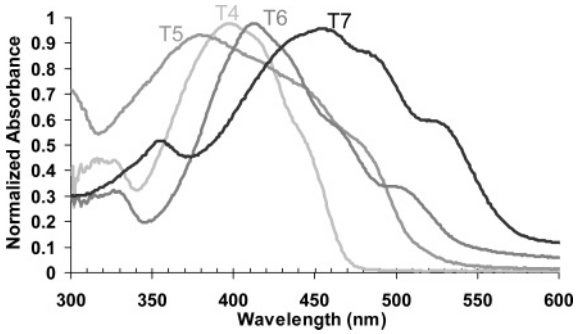

Figure 2. Solid-state UV−vis spectra of the **T4**−**T7** series. **T4**−**T6** display a blue shift in λ_{max} from solution indicating a disruption in planarity, while the **T7** red-shifts slightly. Spectra of all oligomers, but particularly **T7**, have shoulders at higher wavelengths indicative of π interactions in the solid state.

UV−Vis Characterization. The UV−vis spectra of the **T4**−**T7** series in chloroform are shown in Figure 1. The expected bathochromic shift of λ_{max} by about 20 nm per thiophene ring[51] was observed, giving λ_{max} values of 400, 422, 440, and 455 nm for the **T4**−**T7** series, respectively. The solid-state spectra revealed a slightly different trend as shown in Figure 2. In **T4**−**T6**, the λ_{max} values are slightly blue-shifted in the solid state presumably as a result of distortion of the conjugated backbone by the bulky ester end groups. In particular, the **T5** λ_{max} value blue-shifts below that of the **T4**. It is possible that the odd-numbered oligomer is more sensitive to the bulky esters, twisting it farther out of conjugation. However, in contrast, the odd-numbered **T7** exhibits a solid-state λ_{max} value that is comparable to the solution value with shoulders at 480 and 525 nm, which are indicative of intermolecular excitons due to the electronic association of the π orbitals. This result is promising, as this propensity for π-orbital association in the solid state before thermolysis may lead to enhanced order in thin films through partial pre-organization of the molecules. Similarly, the smaller ester moieties on the **T6-acid** precursor allow for π-orbital association in the solid state, as evidenced by the shoulders at 485 and 525 nm (Figure 3). An increase in λ_{max}

(50) Masui, K.; Ikegami, H.; Mori, A. *J. Am. Chem. Soc.* **2004**, *126*, 5074−5075.
(51) Becker, R. S.; Demelo, J. S.; Macanita, A. L.; Elisei, F. *Pure Appl. Chem.* **1995**, *67*, 9−16.

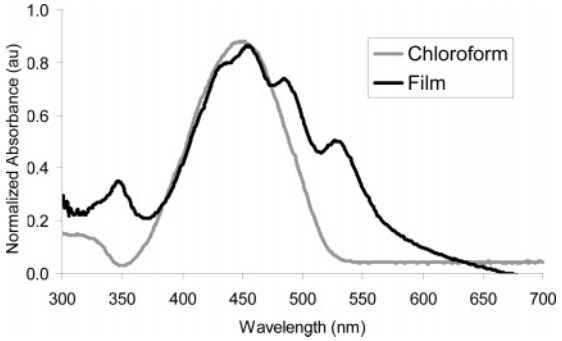

Figure 3. UV-vis spectra of the **T6-acid** precursor in chloroform and in the solid state. The solution λ_{max} of 451 nm shifts slightly to 455 nm in the solid state. Shoulders at 485 and 525 nm indicate the presence of π interactions in the solid state.

in chloroform for the **T6-acid** precursor by about 11 nm over **T6** can be attributed to extended conjugation of the thiophene backbone with the carbonyl groups.

Thermal Characterization. The thermal characteristics of the series were monitored using thermogravimetric analysis (TGA). All data were obtained while heating at 5 °C/min at ambient humidity under a flow of nitrogen gas (see Supporting Information). Thermolysis initiates between 200 and 210 °C in all of the oligomers, but variations are seen in the time required to evaporate the carboxylic acid side product. The TGA instrument is limited in its ability to monitor the progress of this thermolysis reaction because of the high viscosity of the smaller oligomers combined with the low vapor pressure of the acid byproduct. Therefore, additional examination of the products from each TGA sample was done with matrix-assisted laser desorption ionization time-of-flight mass spectrometry. In each case, complete conversion to the bis-alkene or di-acid was confirmed after holding the samples at 200 °C for 30 min, but varying amounts of residual carboxylic acid byproduct were found in each of these samples.

NEXAFS Spectroscopy. To follow the thermolysis reaction more conclusively, thin films of these materials annealed at different temperatures were examined using NEXAFS spectroscopy. The NEXAFS experiments were performed at the NIST/Dow Soft X-ray Materials Characterization Facility of the National Synchrotron Light Source (NSLS) at Brookhaven National Laboratory. NEXAFS is a synchrotron-based photon absorption spectroscopy in which soft X-rays are absorbed to cause resonant excitations of core K or L shell electrons to unoccupied (antibonding) molecular orbitals.[52] Therefore, NEXAFS spectroscopy is element-sensitive by energetic selection of the K-edge accessed and bond-sensitive by the location of the particular transitions within the spectra. The chemical conversion of the molecule from an ester to an alkene during thermolysis can then be characterized by collecting carbon K-edge partial electron yield (PEY) spectra normalized to the total carbon surface signal taken at the orientation-insensitive "magic angle" of 54.7°. PEY spectra were collected at an entrance grid bias of −50 V and represent the chemical structure for a surface-weighted depth of ≈6 nm. We believe that conversion at this depth accurately reflects conversion in the film bulk.

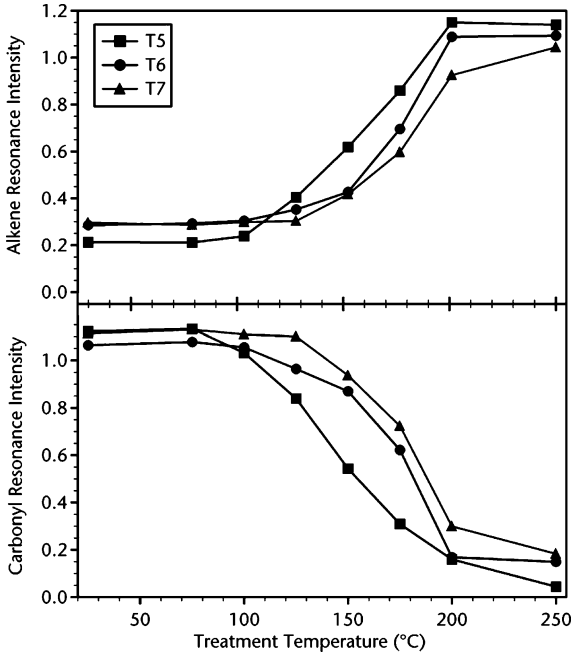

Figure 4. Integrated peak intensities of carbon K-edge NEXAFS spectra quantifying the increasing density of alkene bonds and decreasing density of carbonyl bonds in films of the **T5**−**T7** heated at various temperatures. In all cases, conversion is nearly complete at 200 °C.

Experimental standard uncertainty in peak position for PEY spectra is ±0.1 eV; yield uncertainty is ±2%. Because up to 48 h elapsed between thermal exposure and NEXAFS measurement, samples were checked for aging, but no drift in conversion was observed at room temperature in the dark over several weeks.

The exact conditions used to construct TFT devices were also used to prepare samples for NEXAFS analysis. Films of **T4**−**T7** were spun-cast from chloroform (2−3 mg/mL solutions) on a 100-nm SiO_2 dielectric thermally grown on highly N-doped silicon. The films were divided, subjected to temperatures between 75 and 300 °C for 20 min, and finally cooled to room temperature.

The disappearance of the carbon−oxygen 1s → π^* transition of the ester carbonyl and the appearance of the carbon−carbon 1s → π^* transition of the pendant alkenes were monitored over the range of annealing temperatures.[53−55] The stoichiometric concentrations of these functional groups were quantified by fitting a combination of peak shapes to the spectra and then integrating the peak areas. NEXAFS peaks are typically well-separated in energy and can be deconvoluted by this method. (See Supporting Information for further detail.) As a result of extreme de-wetting from the surface, as discussed below, reliable data for **T4** was unattainable. The combined results for **T5**−**T7** are shown in Figure 4. The unannealed films of **T5**−**T7** exhibit slightly different, low levels of conversion that can be attributed to aging between film casting and the NEXAFS measurement. Thermolysis of **T5** and **T6** initiates around 125 °C, followed by **T7** around 150 °C, as indicated by the increase in the

(52) Stöhr, J. *NEXAFS Spectroscopy*; Springer-Verlag: Berlin, 1992.
(53) Ishii, I.; Hitchcock, A. P. *J. Electron Spectrosc. Relat. Phenom.* **1988**, *46*, 55−84.
(54) Stöhr, J.; Sette, F.; Johnson, A. L. *Phys. Rev. Lett.* **1984**, *53*, 1684−1687.
(55) Urquhart, S. G.; Ade, H. *J. Phys. Chem. B* **2002**, *106*, 8531−8538.

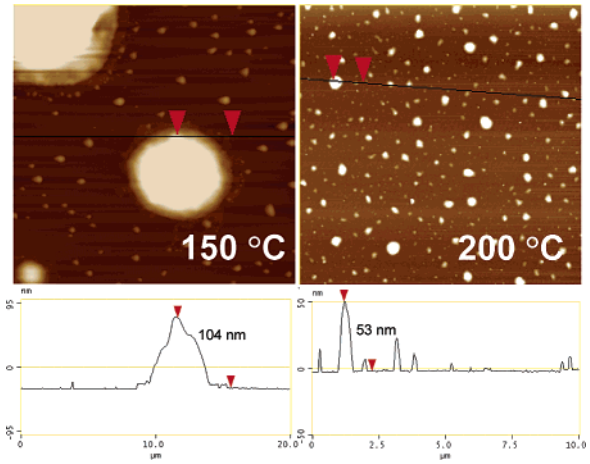

Figure 5. AFM height images (10 × 10 μm) of **T4** spun-cast from chloroform (2−3 mg/mL solutions) on SiO_2 and then heated to the temperatures indicated. Even at low temperature, tall aggregates are formed, resulting in discontinuous films.

alkene intensity and a simultaneous decrease in the carbonyl intensity. These initiation temperatures are lower than those observed in bulk samples possibly because of catalysis by the weakly acidic SiO_2 surface. In the **T5** and **T6** samples, the alkene signal levels off at 200 °C indicating that thermolysis is complete, but the transformation of **T7** requires slightly higher temperatures. The final alkene intensity is consistent with the expected functional group density, being highest for **T5** and lowest for **T7**. The carbonyl signal decrease is also sharp for all three oligomers between 150 and 200 °C as the carboxylic acid byproduct evaporates. However, the evaporation slows from 200 to 250 °C, and the carbonyl signal does not completely disappear in the **T6** and **T7** films until >250 °C. Complete conversion was further confirmed with oxygen K-edge scans by monitoring the ester and the acid byproduct carbonyl resonances (see Supporting Information). In all cases, the ester carbonyl resonance disappears by 200 °C, but a small acid carbonyl resonance remains constant in the **T6** and **T7** films up to 250 °C, finally disappearing by 300 °C. Acid trapping observed by NEXAFS is similar to that observed with TGA, but it occurs to a much lesser extent in thin films. However small, a quantity of trapped acid does remain within the film even though the conversion to the bis-alkene is complete at 200 °C. The effect of the residual acid has yet to be determined and will be the subject of further studies. Further optimization of these materials will incorporate more volatile solubilizing groups, which should help alleviate the problems of residual carboxylic acid in the films.

Film Morphology

Thin films of the materials were spun-cast from chloroform (2−3 mg/mL) onto silicon wafers with a thermally grown 1000-Å SiO_2 layer. Each spun-cast wafer was divided and then heated at 175, 200, 225, or 250 °C for 20 min to investigate the effect of differences in oligomer length as well as thermolysis temperature on film morphology.

AFM Studies. Under all the conditions mentioned above, **T4** was unable to form continuous films after heating of the substrates. As shown in Figure 5, the material seems to clump and de-wet from the surface even at low temperatures. As

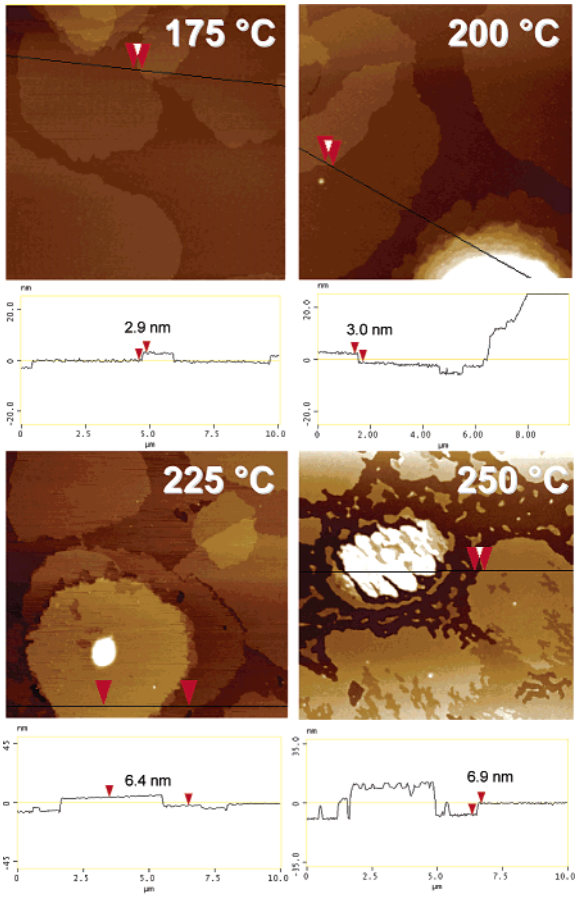

Figure 6. AFM height images (10 × 10 μm) of **T5** films spun-cast from chloroform onto SiO_2 and then heated at the temperature indicated. Large islands with monolayer high terraces dramatically increase in height with increasing temperatures. While films heated to 225 °C remain continuous, heating to 250 °C causes the films to crack and de-wet from the surface.

the temperature increases, the large 5−10 μm clumps seen at 150 °C disperse into smaller islands approximately 500 nm in width.

The behavior of **T5** is very similar that of the previously studied **T6**.[48,49] Upon the application of heat, crystalline terraced structures form with step heights of about 3 nm, corresponding to the long axis of the molecule (Figure 6). As is the case for **T6**, after thermal release of the bulky solubilizing groups the molecules undergo a drastic reorganization and orient themselves perpendicular to the surface. The diameter of the terraced islands is larger than that seen for **T6**, and the height of the islands increases much more dramatically above 200 °C. A continuous film, at least one monolayer thick, persists up to 225 °C, but significant cracking and de-wetting from the SiO_2 surface is seen when heated to 250 °C. Evidence for the presence of at least a monolayer below 225 °C can be seen in the phase images shown in Figure 7. Phase images of films heated at 200 °C are monochromatic suggesting the presence of only one phase and indicate that the tip of the atomic force microscope is only encountering one type of material, namely, the **T5** molecules. In contrast, the phase image of a film heated to 250 °C shows two distinct phases, which can be interpreted as **T5** and the SiO_2 surface below. This de-wetting was not observed at these temperatures with films of the corresponding **T6** oligomer.

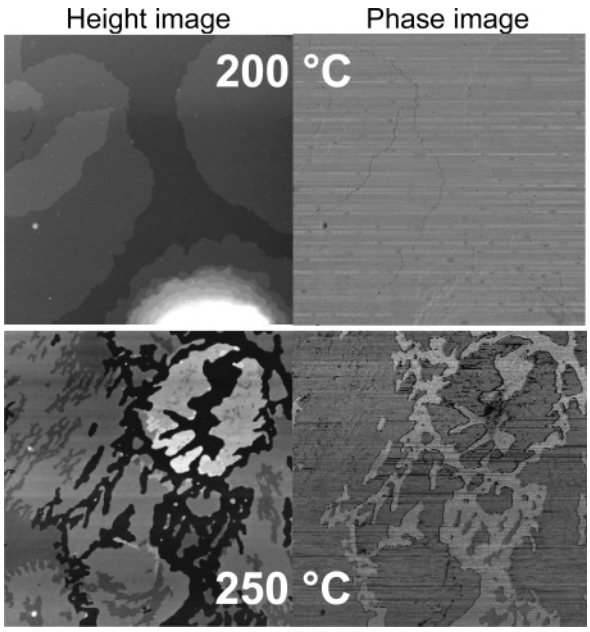

Figure 7. AFM height images (10 × 10 μm) of films of **T5** spun-cast from chloroform onto SiO_2. The phase image of a film heated at 200 °C is monochromatic, indicating that the AFM tip is encountering only one type of surface. However, a color change can be seen in the phase image of a film heated at 250 °C, confirming that the film is de-wetting, revealing the SiO_2 below.

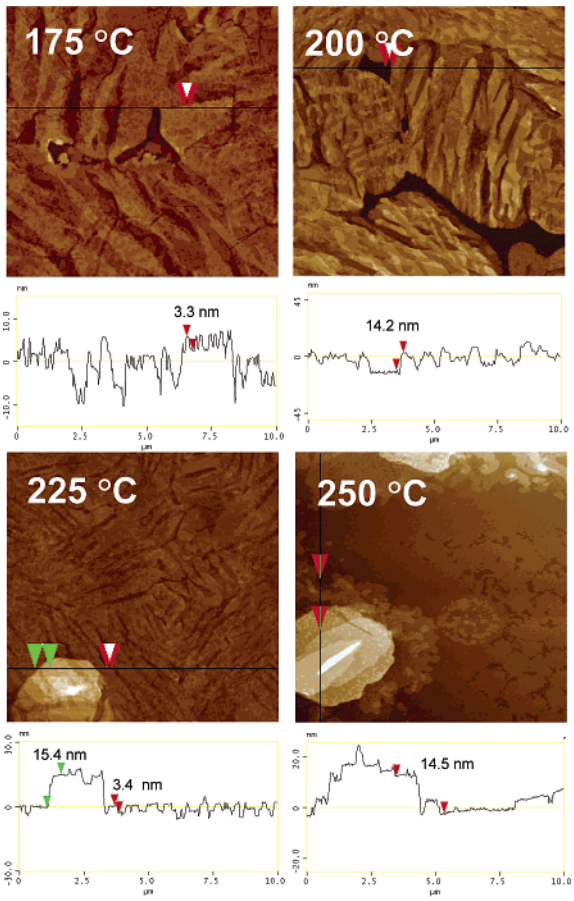

Figure 8. AFM height images (10 × 10 μm) of **T7** heated at the temperatures indicated. Islandlike terraces are not seen until films are heated to 225 °C. Unlike the smaller oligomers, no cracking or de-wetting is observed up to 250 °C.

AFM images of the **T7** films are shown in Figure 8. These films show a substantial change in morphology as compared

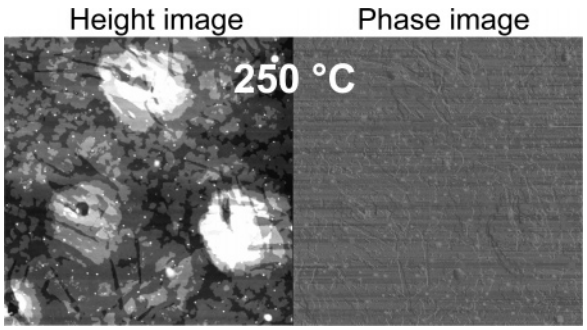

Figure 9. AFM height and phase images (10 × 10 μm) of a **T7** film spun-cast on SiO_2. The phase image of a film heated at 250 °C is still monochromatic, indicating that the film is not de-wetting.

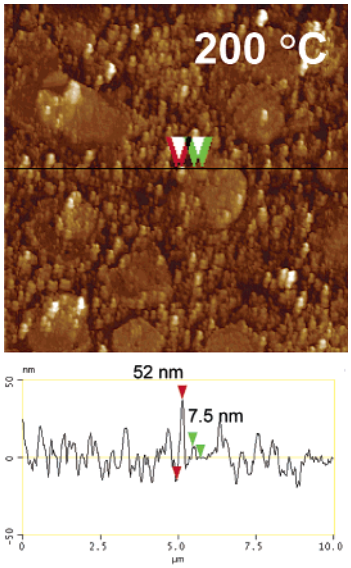

Figure 10. AFM height and phase images (10 × 10 μm) of a **T6-acid** precursor film spun-cast from SiO_2 then heated to 200 °C. At all annealing temperatures films are amorphous with small regions of aggregation.

to films of the **T5** and **T6**. Crystalline films are observed at all annealing temperatures, but terraced island formation is not seen until the temperatures exceed 225 °C. These films are also less susceptible to de-wetting, as revealed in the phase images of films heated at 250 °C, shown in Figure 9. The phase image remains monochromatic indicating that the AFM tip is only encountering the **T7** molecules and not the SiO_2 below.

As expected, the **T6-acid** precursor generated a much different morphology than that seen in **T5**−**T7**. As shown in Figure 10, the **T6-acid** seems to have good surface coverage after thermolysis, but the films are highly disordered. Small regions of aggregation can be discerned, but no order within the aggregates can be found. The pendant carboxylic acids are clearly affecting the molecular ordering, with hydrogen bonding between molecules perhaps competing or taking precedence over π-stacking interactions.

NEXAFS Evaluation. To further quantify the amount of de-wetting or cracking of the thin films at various temperatures, NEXAFS spectroscopy was employed. All of the oligomers were spun-cast from chloroform (2−3 mg/mL) onto SiO_2, which exhibits a prominent oxygen−silicon σ^* resonance in the oxygen K-shell spectra. Calibration of the spectra versus bare SiO_2 allows determination of the fraction of organic film within ~6 nm of the sampling depth. AFM

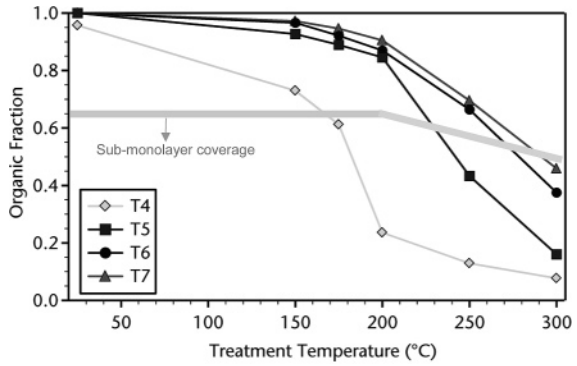

Figure 11. Fraction of the **T4**−**T7** oligomers within 6 nm of the surface of the film when heated at various temperatures. Values are calculated from NEXAFS oxygen K-shell spectra, in which the oxygen−silicon σ^* resonance of SiO_2 can be used to quantify exposure of the dielectric below. The oligomers range in length from 2 to 3 nm and the measurement samples to a depth of 6 nm; therefore, monolayer coverage remains intact until the organic/SiO_2 ratio drops below 35, 40, 45, or 50% for the **T4**−**T7** series, respectively.

images confirm that the molecules orient with the long axis perpendicular to the surface, and as a result of this orientation, the height of a single monolayer ranges from about 2.1 nm for **T4** to 3.1 nm for **T7**. Therefore, the point at which the average thickness of the film drops below a monolayer, indicating de-wetting, should coincide with the point at which the SiO_2 signal is detected within 2−3 nm of the surface of the film.

As shown in Figure 11, these values are given as a ratio of organic to (SiO_2 + organic), where a value of 1 would indicate that there is no SiO_2 within 6 nm of the surface and a value of 0 would be a surface of entirely SiO_2. (See Supporting Information for further detail.) Because the materials vary in height, the films lose continuity when the fractions of the organic film drops below 35, 40, 45, or 50% for the **T4**−**T7** series, respectively.

The trend seen in Figure 11 correlates well with the AFM images discussed earlier. **T4** begins to lose coverage almost immediately, and the average film thickness becomes submonolayer as the temperature reaches 175 °C. The **T5**−**T7** series exhibits a closer trend, where no SiO_2 is detected until the onset of thermolysis between 150 and 200 °C. As the molecules order and coalesce into the tall structures seen in the AFM images, the average film thickness becomes less than the sampled depth. The series follows the expected trend where **T5** loses continuity first around 240 °C, followed by **T6** around 275 °C, and finally the **T7** average film thickness becomes submonolayer around 300 °C.

The trends in film morphology of the **T4**−**T7** series can be summarized as follows. Because the molecules contain no surface specific self-assembling functionalities, the main driving forces for assembly in these materials are thought to be the $\pi-\pi$ interactions between the conjugated oligomers and the surface interactions of the underlying substrate. The temperatures required for the chemical conversion of these molecules from their soluble ester form to the corresponding insoluble alkene form contribute a significant source of kinetic energy to the molecules allowing for drastic reorganization to take place. As the smallest oligomer, **T4** is, therefore, most affected by the thermal energy, allowing the molecules to overcome the substrate surface energy more easily and clump and de-wet from the surface. This de-wetting is also seen in the **T5**, but only at temperatures >225 °C. This trend continues in the longer oligomers, where temperatures in excess of 250 °C are needed to see cracking in the **T6** films while no de-wetting is seen until the temperature reaches 300 °C for **T7**. Increasing the oligomer size increases the activation energy and, thus, restricts movement, resulting in continuous films at higher temperatures. This increase in size also leads to an increased barrier for perpendicular alignment of the molecules with the surface. Significant changes in film morphology are not seen for the largest oligomer by AFM observation until temperatures in excess of 225 °C are reached. These trends are supported by the charge mobility data that is presented below. The **T7** molecules need temperatures in excess of 225 °C to rearrange into their optimal π networks resulting in the highest charge mobility.

Table 1. Average Hole Mobilities, Measured over 10 or More Devices, and On/Off Ratios for OTFT Devices of the T4−T7 Series at the Given Temperatures[a]

	175 °C		200 °C		225 °C		250 °C	
	μ	on/off	μ	on/off	μ	on/off	μ	on/off
T4	10^{-5}	10^2	10^{-6}	10				
T5	0.013	10^4	0.018	10^4	0.0063	103	10^{-7}	<10
T6	0.013	10^4	0.038	10^6	0.014	106	0.011	10^5
T7	0.011	10^4	0.028	10^6	0.044	105	0.031	10^5

[a] Units for μ are $cm^2/(V\cdot s)$.

The determination of the crystal lattice spacing of the individual molecules in these terraced films would have been useful, but we have been unable to ascertain these parameters by standard X-ray diffraction techniques because the films are ultrathin. However, we are able to observe a single diffraction peak in the annealed films, indicating that the films are indeed crystalline.[48] Further information about orientation and ordering of the molecules within the films was obtained using multi-angle NEXAFS spectroscopy, which was published elsewhere.[56]

Electrical Characterization

Organic thin film transistor (OTFT) devices were fabricated on low resistivity n-type silicon wafers, using 1050 Å of thermally grown SiO_2 as the dielectric, in top-contact geometry. The active semiconducting layer was applied by spin-casting 2−3 mg/mL solutions of the oligomers in chloroform, and the films were then annealed at temperatures between 175 and 250 °C in a nitrogen atmosphere. Gold contacts were patterned on top of the films using various shadow masks giving channel lengths from 5 to 40 μm and widths from 200 to 400 μm. All devices were tested as p-type OTFTs in the accumulation regime, and saturation mobilities were calculated using the equation $\mu = gm^2/2I_DC_{ox}(W/L)$.

Devices annealed at temperatures between 175 and 250 °C were tested at various intervals. The averages measured over 10 or more devices for each of the materials tested are summarized in Table 1. In all cases, the standard deviation

(56) DeLongchamp, D.; Sambasivan, S.; Fischer, D. A.; Lin, E. K.; Chang, P.; Murphy, A. R.; Fréchet, J. M. J.; Subramanian, V. *Adv. Mater.* **2005**, *17*, 2340−2344.

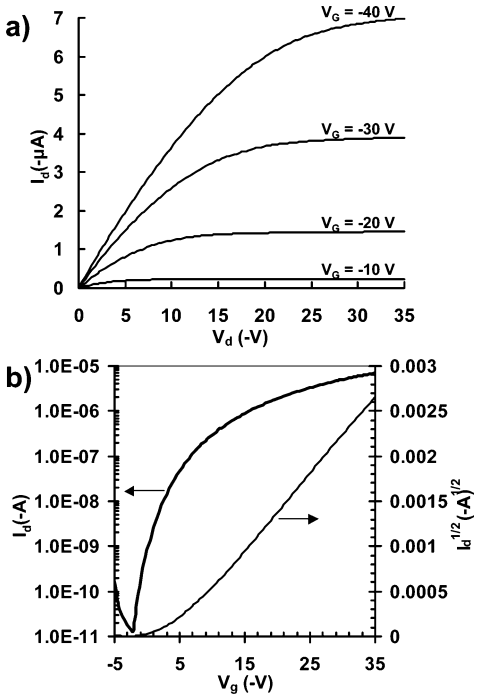

Figure 12. Electrical characterization of a **T7** film after heating to 225 °C. (a) Drain current I_D vs drain voltage V_D as a function of gate voltage for a top-contact device with $L = 200$ μm and $W = 20$ μm (dielectric = 1050 Å). (b) Drain current and the square root of the drain current versus gate voltage at $V_D = -35$ V.

was less than ±0.01. All top-contact devices tested prior to heat treatment yielded low field effect mobilities in the range of 10^{-5} cm^2/(V·s) with on/off ratios from 10 to 100.

As expected from the poor film quality of **T4**, none of the devices tested exhibited significant semiconducting behavior. The highest measured mobilities were on the order of 10^{-5} cm^2/(V·s) and were similar to or worse than those of the unannealed samples.

The OTFT performance trends in **T5** correlated well with the observed film morphology. At temperatures below 200 °C, good device performance was observed with mobilities reaching 0.02 cm^2/(V·s) [average = 0.01 cm^2/(V·s)] with on/off ratios $>10^4$. A small drop in performance is seen when devices were heated to 225 °C, and a complete loss of conductivity is seen at 250 °C as a consequence of film dewetting.

The device performance from spun-cast films of the **T6** peaks around 200 °C,[48] giving measured mobilities up to 0.05 cm^2/(V·s) [average = 0.038 cm^2/(V·s)]. Slightly higher maximum mobilities of 0.06 cm^2/(V·s) [average = 0.044 cm^2/(V·s)] can be achieved in spun-cast films of **T7**, but when annealed at temperatures >225 °C. The trend of mobility versus annealing temperature closely follows film morphology, as **T6** is able to rearrange into the well-organized, terraced structures at a lower temperature than **T7**. Current−voltage characteristics of a typical **T7** film heated to 225 °C are shown in Figure 12. These plots are similar to those obtained for **T5** and **T6**.

While slight differences between the even- and the odd-numbered oligomers exist in the UV and thermal characteristics, we do not observe any odd−even effects in the charge mobilities. The mobility for each oligomer seems to scale with increasing number of thiophene units, which is similar to the findings for a series of thermally evaporated unsubstituted thiophene oligomers.[57]

The mobilities measured with these materials are noteworthy given the average film thicknesses measured with AFM and NEXAFS spectroscopy. These materials appear to perform best when the average film thickness is roughly equal to that of a single monolayer. Many studies have shown that the majority of the charge carriers are located within the first one or two molecular layers of material located adjacent to the dielectric layer.[58,59] However, because it is very difficult to obtain a defect-free monolayer using typical evaporation techniques, multilayers must usually be deposited to achieve maximum charge mobilities. In our system, spun-cast oligothiophenes can self-assemble into very thin films that are unprecedented in the literature, resulting in the efficient charge mobility rarely seen to occur in such thin films. Limiting the amount of material deposited on the surface using ink-jet printing can further control the morphology of these films.[48,60] We have found that uniform monolayers of **T6** and films less than three layers thick of **T7** can be deposited by this method. In all cases, the films with controlled thickness exhibit higher field-effect mobility than the spun-cast films presumably due to increased molecular order within the films. Minimizing the thickness of the semiconductor film is also beneficial to the electrical performance by improving gate control of the channel, and reducing undesired source to drain leakage at low gate bias. We have also found that devices made from thinner films exhibit minimal hysteresis as a result of reduced charge trapping within the film.[60] Further aspects of this phenomenon are currently under investigation.

Conclusion

Overall, this study highlights the interplay between the various forces that are involved in the self-assembly of continuous organic thin films. Adjusting the length or end functionalization of the oligomers, the strength of the $\pi-\pi$ interactions, and the ability of the molecules to form hydrogen bonds all had significant effects on the final morphology of the molecules. While oligomer length modifications led to predictable and controlled changes in processed films, replacing the alkene end groups with carboxylic acids caused drastic differences in morphology and performance. This work also shows that oligomer length in solution-processed films can be exploited to achieve the desired properties. The tradeoff between surface coverage and applied temperature may be particularly important when tailoring molecules for use on various substrates with different surface energies. This study, therefore, emphasizes the necessity to balance the ability of the material to self-assemble while still maintaining surface coverage. This balance in self-assembly from a solution-based process will

(57) Nagamatsu, S.; Kaneto, K.; Azumi, R.; Matsumoto, M.; Yoshida, Y.; Yase, K. *J. Phys. Chem. B* **2005**, *109*, 9374−9378.
(58) Dinelli, F.; Murgia, M.; Levy, P.; Cavallini, M.; Biscarini, F.; de Leeuw, D. M. *Phys. Rev. Lett.* **2004**, *92* (11).
(59) Dodabalapur, A.; Torsi, L.; Katz, H. E. *Science* **1995**, *268*, 270−271.
(60) Chang, P. C.; Molesa, S. E.; Murphy, A. R.; Fréchet, J. M. J.; Subramanian, V. *62nd DRC Conference Digest* **2004**, *1*, 183−184.

play a key role in optimizing semiconductor properties for materials designed for use in low-cost and low-temperature applications.

Acknowledgment. Financial support of this work by the Department of Energy (DE-AC03-76SF00098) under the plastic electronics program at LBNL is gratefully acknowledged. Thanks are also due for additional support by NSF, the Eastman-Kodak Co., MARCO, and the NRC-NIST postdoctoral fellowship program (for D.M.D.).

Supporting Information Available: Complete experimental procedures and characterization of **2**−**5**, **T4**, **T5**, **T7**, and **T6-acid** precursor as well as all OTFT fabrication procedures. This material is available free of charge via the Internet at http://pubs.acs.org.

CM0515350